



Published in final edited form as:

Int J Parasitol. 2018 April ; 48(5): 359–369. doi:10.1016/j.ijpara.2018.01.002.

***Heligmosomoides polygyrus* Venom Allergen-like Protein-4 (HpVAL-4) is a sterol binding protein**

Oluwatoyin A. Asojo^{a,*}, Rabih Darwiche^b, Selam Gebremedhin^a, Geert Smant^c, Jose L. Lozano-Torres^c, Claire Drurey^d, Jeroen Pollet^a, Rick M. Maizels^d, Roger Schneider^b, and Ruud H. P. Wilbers^c

^aNational School of Tropical Medicine, Baylor College of Medicine, Houston, TX 77030, USA

^bDivision of Biochemistry, Department of Biology, University of Fribourg, Chemin du Musée 10, CH 1700 Fribourg, Switzerland ^cLaboratory of Nematology, Wageningen University, Droevendaalsesteeg 1, 6708 PB, Wageningen, The Netherlands ^dWellcome Centre for Molecular Parasitology, Institute for Infection, Immunity and Inflammation, University of Glasgow, Sir Graeme Davies Building, 120 University Place, Glasgow G12 8TA, UK

Abstract

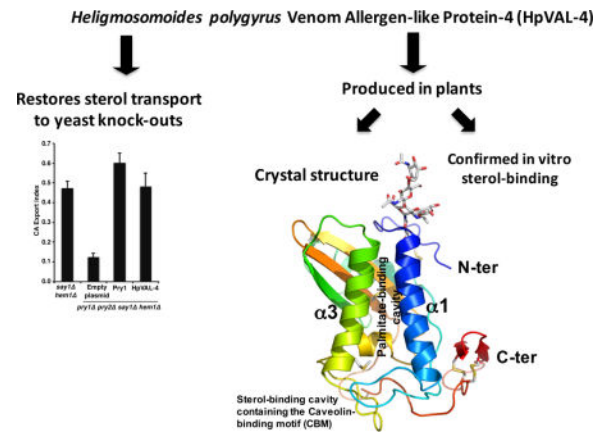
Heligmosomoides polygyrus bakeri is a model parasitic hookworm used to study animal and human helminth diseases. During infection, the parasite releases excretory/secretory (ES) products that modulate the immune system of the host. The most abundant protein family in ES products comprises the venom allergen-like proteins (VALs), which are members of the SCP/TAPS (Sperm-coating protein / Tpx / antigen 5 / pathogenesis related-1 / Sc7) superfamily. There are >30 secreted *Heligmosomoides polygyrus* VAL proteins (HpVALs) and these proteins are characterized by having either one or two 15 kDa CAP (cysteine-rich secretory protein (CRISP) / antigen 5 / pathogenesis related-1) domains. The first known HpVAL structure, HpVAL-4, refined to 1.9 Å is reported. HpVAL-4 was produced as a homogeneously glycosylated protein in leaves of *Nicotiana benthamiana* infiltrated with recombinant plasmids, making this plant expression platform amenable for the production of biological products. The overall topology of HpVAL-4 is a three layered $\alpha\beta\alpha$ sandwich between a short N-terminal loop and a C-terminal cysteine rich extension. The C-terminal cysteine rich extension has two strands stabilized by two disulfide bonds and superposes well with the previously reported extension from the human hookworm *Necator americanus* Ancylostoma secreted protein-2 (Na-ASP-2). The N-terminal loop is connected to alpha helix 2 via a disulfide bond previously observed in Na-ASP-2. HpVAL-4 has a central cavity that is more similar to the N-terminal CAP domain of the two CAP Na-ASP-1 from *Necator americanus*. Unlike Na-ASP-2, mammalian CRISP, and the C-terminal CAP domain of Na-ASP-1, the large central cavity of HpVAL-4 lacks the two histidines required to coordinate divalent cations. HpVAL-4 has both palmitate-binding and sterol-binding cavities and is able to

*Corresponding author. Oluwatoyin A. Asojo, National School of Tropical Medicine, Baylor College of Medicine, 1102 Bates Av Houston TX 77030, USA, Tel.: +1 832 8240533. asojo@bcm.edu.

Publisher's Disclaimer: This is a PDF file of an unedited manuscript that has been accepted for publication. As a service to our customers we are providing this early version of the manuscript. The manuscript will undergo copyediting, typesetting, and review of the resulting proof before it is published in its final citable form. Please note that during the production process errors may be discovered which could affect the content, and all legal disclaimers that apply to the journal pertain.

complement the in vivo sterol export phenotype of yeast mutants lacking their endogenous CAP proteins. More studies are required to determine endogenous binding partners of HpVAL-4 and unravel the possible impact of sterol binding on immune-modulatory functions.

Graphical abstract



Keywords

Sperm coating protein (SCP); Testis specific proteins (Tpx); Pathogenesis related-1 (PR-1); Cysteine-rich secretory protein (CRISP); Venom antigen 5; Excretory-secretory products; Sterol binding

1. Introduction

Heligmosomoides polygyrus bakeri is a rodent intestinal nematode that is closely related to ruminant and human hookworm parasites. *Heligmosomoides polygyrus* is able to survive long-term in the murine host, and is in widespread use as a model for chronic nematode infections (Behnke, 1987; Robinson et al., 1989). More importantly, *H. polygyrus* has been used as a model to study immunological processes involved in chronic parasitic nematode infections and to characterize host-parasite relationships for over three decades (Behnke, 1987; Robinson et al., 1989; Behnke et al., 2009; Reynolds et al., 2012; Harris et al., 2014). *Heligmosomoides polygyrus* is retained in the intestine and elicits strong systemic T_H2 cell responses (Svetic et al., 1993; Wahid et al., 1994). It was also determined that *H. polygyrus* infection drives expansion of regulatory T cells which are able to suppress allergic airway inflammation in mouse models of allergic inflammation (Finney et al., 2007; Rausch et al., 2008; Smith et al., 2016).

Additionally, *H. polygyrus* secretes immune-modulatory factors and effectors that may account for both immune evasion and suppression evident during infection. Many of the immunomodulatory molecules are released as parasite excretory/secretory (ES) products (Hewitson et al., 2009; Johnston et al., 2009; Ferreira et al., 2013). Passive immunization with antisera to these ES products confers 50–75% protection against challenge infection (Hewitson et al., 2009). Due to their immunomodulatory properties, ES products from *H. polygyrus* have been explored as putative therapeutic agents for autoimmune and allergic

diseases (Harris et al., 2014). Similarly, ES products have been studied as candidate vaccine antigens for hookworm infection and schistosomiasis (Verjovski-Almeida et al., 2003; Bethony et al., 2005; Fujiwara et al., 2005).

Proteomic analysis of ES products of adult *H. polygyrus* revealed that the most abundant proteins are members of the venom allergen-like protein (VAL) family, and among the major ones is *H. polygyrus* VAL-4 (HpVAL-4) (Hewitson et al., 2011b). It was previously shown that homologues of VALs known as *Ancylostoma* secreted proteins (ASPs) are the predominant molecules secreted by canine and human hookworms (Cantacessi et al., 2010; Wang et al., 2010b). The immunomodulatory functions of ASPs are well characterized and some are being explored as vaccines and adjuvants (Fujiwara et al., 2005; He et al., 2009; Gonzalez-Hernandez et al., 2016). VALs are members of the superfamily that is known as CAP (cysteine-rich secretory protein / antigen 5 / pathogenesis related-1) or SCP/TAPS (Sperm-coating protein / Tpx / antigen 5 / pathogenesis related-1 / Sc7). The CAP domain (Pfam PF00188) has been implicated in conditions requiring cellular defense or proliferation including plant responses to pathogens and human brain tumor growth (Hawdon et al., 1999; Ding et al., 2000; Gao et al., 2001; Zhan et al., 2003; Gibbs et al., 2008). In the case of parasite-encoded CAP proteins, many are considered to fulfill immune modulatory functions to sustain survival in the host, and for the same reason are attractive targets for vaccine-induced anti-parasite immunity (Cantacessi et al., 2009).

There are over 30 secreted HpVALs which dominate the immune response in *H. polygyrus* infected mice (Hewitson et al., 2011b). Additionally, as observed in human and canine hookworms, HpVALs are characterized by having either a single or double 15 – 25 kDa CAP domain. In infected mice, the antibody response primarily targets four HpVALs, the double-domain HpVAL-1, -2 and -3, and the single domain HpVAL-4. Following secondary infection of mice, antibodies are directed at the same four HpVALs as well as another single domain family member, HpVAL-7. Both HpVAL-1 and HpVAL-2 bear an immunodominant *O*-linked glycan which is exposed on the parasite surface (Hewitson et al., 2011a). Interestingly, each member of the HpVAL family has a distinct pattern of expression during the parasite life cycle with HpVAL-4 being expressed at high levels by all mammalian stages from day 3 and day 5 p.i, L3s, L4s, and adult worms (Hewitson et al., 2013)

Several structures of proteins having a single CAP domain and one structure of a hookworm ASP with two CAP domains have been reported (Fernandez et al., 1997; Serrano et al., 2004; Asojo et al., 2005; Guo et al., 2005; Shikamoto et al., 2005; Wang et al., 2005; Gibbs et al., 2008; Asojo, 2011; Xu et al., 2012; Borloo et al., 2013). Each CAP domain has a large central cavity (Serrano et al., 2004; Asojo et al., 2005, 2011; Gibbs et al., 2008; Suzuki et al., 2008; Wang et al., 2010a; van Galen et al., 2012; Xu et al., 2012; Mason et al., 2014; Darwiche et al., 2016; Baroni et al., 2017). The function of the cavity is unknown but in some SCP/TAPS proteins the cavity contains two histidine residues that have been shown to bind divalent cations including Zn^{2+} and Mg^{2+} (Gibbs and O'Bryan, 2007; Gibbs et al., 2008). The ability to bind Zn^{2+} is critical for heparin-sulfate dependent inflammatory mechanisms of the cobra SCP/TAPS protein natrin (Wang et al., 2010a).

The central CAP domain has a conserved alpha-beta-alpha sandwich topology with variations in the lengths of their strands and helices as well as the lengths, orientations, and locations of loops (Asojo, 2011). These long flexible loops make up as much as 50% of the overall structure of the CAP domain, making it difficult to accurately predict or model their structures (Asojo et al., 2005; Asojo, 2011; Darwiche et al., 2016; Baroni et al., 2017). Interestingly, one of the flexible loop regions of the CAP domain was identified as the sterol-binding caveolin-binding motif (CBM) of yeast CAP proteins required for in vivo cholesterol transport (Choudhary et al., 2014; Darwiche et al., 2016). Two additional lipid-binding regions have been identified in CAP proteins, and all three lipid-binding regions are unique and unconnected in all reported monomer structures of CAP domains (Fernandez et al., 1997; Hawdon et al., 1999; Ding et al., 2000; Gao et al., 2001; Zhan et al., 2003; Serrano et al., 2004; Asojo et al., 2005; Guo et al., 2005; Shikamoto et al., 2005; Wang et al., 2005; Gibbs et al., 2008; Asojo, 2011; Xu et al., 2012; Borloo et al., 2013). The second lipid-binding region is a large hydrophobic cavity between two helices that was identified in horsefly tablysin-15. Tablysin-15 binds leukotrienes in this cavity and functions as an anti-inflammatory scavenger of eicosanoids (Xu et al., 2012). In addition, the yeast CAP protein Pry1 is structurally able to accommodate lipids such as palmitate, and it binds and exports fatty acids similarly to tablysin-15 (Darwiche et al., 2017). The third lipid-binding motif has only been reported on the surface of human Golgi-associated PR-1 protein (GLIPR2) and facilitates the binding of up to three phosphatidylinositol molecules (van Galen et al., 2010, 2012). These structural and functional insights into the SCP/TAPS proteins from many different organisms prompted us to analyze a predominant homologue secreted into *H. polygyrus* ES products, HpVAL-4, and we present here the X-ray structure and functional role of HpVAL-4 in cholesterol transport.

2. Materials and methods

2.1. Plant-based expression of HpVAL-4

The complete sequence encoding mature HpVAL-4 was codon optimized in-house and synthetically constructed at GeneArt. This sequence was cloned into a pHYG expression vector and was preceded by the *Arabidopsis thaliana* chitinase signal peptide (cSP). The HpVAL-4 expression vector was used to transform *Agrobacterium tumefaciens* (strain MOG101) and used for agro-infiltration. To enhance expression, the plasmid vector pBIN61 containing the silencing inhibitor p19 from tomato bushy stunt virus was co-infiltrated. HpVAL-4 and p19 *Agrobacterium tumefaciens* clones were grown in Lennox broth (10 g/L of peptone, 5 g/L of yeast extract, 10 g/L of NaCl pH 7.0) containing 50 µg/ml of kanamycin and 20 µM acetosyringone for 16 h at 28 °C/250 rpm. For agro-infiltration of HpVAL-4 and p19, MMA infiltration medium (20 g/L of sucrose, 5 g/L of Murashige and Skoog basal salt mixture, 1.95 g/L of (*N*-morpholino)ethanesulfonic acid pH 5.6) containing 200 µM acetosyringone was used to suspend the bacterial cultures to a final O.D. of 0.5 per culture. A 1 ml needleless syringe was used to infiltrate the *Agrobacterium* suspension into the youngest fully expanded leaves of 5–6 weeks old *Nicotiana benthamiana* plants at the abaxial side. *Nicotiana benthamiana* plants were maintained in a controlled greenhouse compartment (UNIFARM, Wageningen, Netherlands) and infiltrated leaves were harvested at 5–6 days post infiltration.

2.2. Purification of HpVAL-4

HpVAL-4 was purified from the leaf extracellular space (apoplast) as described previously (Wilbers et al., 2017). Briefly, the infiltrated leaves were submerged in ice-cold extraction buffer (20 mM sodium citrate pH 3.6, 100 mM NaCl and 0.1% v/v Tween-20). The submerged leaves were vacuum infiltrated and the apoplast fluid was retrieved by centrifugation for 10 min at 2000 *g*. The apoplast fluid was clarified by centrifugation for 5 min at 16,000 *g*. HpVAL-4 was then purified from the apoplast fluid using HS POROS 50 strong cation exchange (CEX) resin (Applied Biosystems, USA). Prior to purification the apoplast fluid was passed over a G25 sephadex column with CEX binding buffer (20 mM sodium citrate buffer pH 3.6, 100 mM NaCl). HpVAL-4 bound to CEX resin was eluted with 20 mM Tris-HCl buffer pH 9.0 containing 2M NaCl. The purification was performed on an ÄKTA Prime Chromatography System (GE Healthcare, USA) using a constant flow rate of 10 mL/min for binding and washing, and 2 mL/min for elution. Eluted HpVAL-4 was dialyzed overnight in PBS. Recombinant HpVAL-4 was separated under reduced conditions by SDS-PAGE on a 12% Bis-Tris gel (Invitrogen, USA) and subsequently stained with Coomassie brilliant blue staining.

2.3. Analysis of N-glycan composition

For N-glycan analysis, 1–2 µg of purified HpVAL-4 was reduced and denatured for 10 min at 95 °C in PBS containing 1.3% (w/v) SDS and 0.1% (v/v) β-mercaptoethanol. SDS was neutralized by adding 2% (v/v) NP-40 prior to overnight digestion at 37°C with trypsin (Sigma-Aldrich, USA) immobilized to N-hydroxysuccinimide-activated sepharose (GE Healthcare). Trypsin beads were removed from the digestion mix by centrifugation and the pH of the mix was adjusted to 5 using 1 M sodium acetate. PNGase A (0.5 mU; Roche, Switzerland) was used to release N-glycans from HpVAL-4 while incubating overnight at 37°C. The incubation mixture was applied to C18 Bakerbond™ SPE cartridges (JT Baker, USA) and the N-glycans were extracted from the flow-through on Extract Clean™ Carbo SPE columns. Eluted N-glycans were labeled with anthranilic acid (Sigma-Aldrich) and desalted by hydrophilic interaction chromatography on Biogel P10 (BioRad). Samples in 75% acetonitrile were mixed with 1 µl of matrix solution (20 mg/ml of 2,5-dihydroxybenzoic acid in 50% acetonitrile, 0.1% (v/v) trifluoroacetic) and were dried under a stream of warm air. Matrix-assisted laser desorption/ionization (MALDI) time-of-flight mass spectra (MS) were obtained using an Ultraflex II mass spectrometer (Bruker Daltonics, USA).

2.4. Crystallization

HpVAL-4 (10 mg/ml) in PBS was screened for crystallization conditions with commercial screens from Qiagen (Germany), Hampton Research (USA) and Microlytics (USA). Crystals were obtained from multiple conditions with polyethylene glycol, and the best diffracting crystals were obtained at 298 K by vapor diffusion in sitting drops by mixing 1.5 µL of protein solution with an equal volume of the reservoir solution containing 0.1 M sodium acetate trihydrate at pH 4.5, 22.5% (w/v) polyethylene glycol 0.3 – 8 kD. Since the crystals grew in solutions that contained adequate cryo-protectant, all crystals were flash-cooled directly in a stream of N₂ gas at 113 K prior to collecting diffraction data.

2.5. Data collection and structure determination

X-ray diffraction data were collected at the Baylor College of Medicine, USA, core facility using a Rigaku HTC detector. The X-ray source was a Rigaku FR-E+ SuperBright microfocus rotating anode generator with VariMax HF optics. A data set was collected from a single crystal with a crystal-to-detector distance of 105 mm and exposure times of 120 s for 0.5° oscillations, using the Crystal Clear (d*trek) package (Pflugrath, 1999). Data was processed using MosFLM (Leslie, 2006). The crystal belonged to the triclinic space group P_1 with cell constants $a=49.5596 \text{ \AA}$ $b=61.5645 \text{ \AA}$ $c=74.8188 \text{ \AA}$, $\alpha=111.595^\circ$ $\beta=90.14^\circ$ $\gamma=113.475^\circ$.

Similar to previous CAP structures, HpVAL-4 structure was solved after several attempts at molecular replacement (MR) using different search models (Asojo et al., 2005; Asojo, 2011) with PHASER (Storoni et al., 2004; McCoy et al., 2005). Using Na-ASP-2 as the search model, a solution was obtained and the model was improved through automatic model building with ARP/wARP (Morris et al., 2003, 2004) followed by manual model building cycles using the program Coot (Emsley et al., 2010) and structure refinement with REFMAC5 (Murshudov et al., 2011) within the CCP4 package (Winn et al., 2011) and Phenix (Terwilliger et al., 2008; Adams et al., 2010). The resulting model was comprised of amino acid residues, glycans, and water molecules. No electron density was observed that could be modeled as any lipids usurped during recombinant protein production. Ribbon diagram and model figures were generated using PyMOL (www.pymol.org, Delano, 2002). Details of the quality of the structure as well as data collection are shown in Table 1. The atomic coordinate and structure factors have been deposited in the protein databank (www.rcsb.org) under accession number 5WEE.

2.6. Size exclusion chromatography and multi-angle light scattering (SEC-MALS)

SEC-MALS experiments were performed by loading ~10 μg of protein sample onto a Phenomenex Yarra 3 μm SEC-2000 column (Phenomenex, Torrance, CA, USA) at a flow-rate of 0.5 ml/min using an Agilent 1260 Infinity series HPLC. The mobile phase was PBS buffer at pH 7.4. The elution was detected with a UV detector (Agilent, USA) a miniDAWN triple-angle light-scattering detector (Wyatt Technology, USA) and with an Optilab rEX differential refractometer (Wyatt Technology) connected in series. The isotropic scatterer for detector normalization was bovine serum albumin. Since the light scattered by a protein is directly proportional to its weight-average molecular mass and concentration, molecular masses were calculated from the light-scattering and interferometric refractometer data using ASTRA 6.1 software.

2.7. In vivo sterol export from mutant yeast cells

Acetylation and export of sterols into the culture supernatant was examined as previously described (Tiwari et al., 2007). Heme (*hem1*) -deficient yeast cells were cultivated in presence of Cholesterol/Tween 80 containing media and labeled with 0.025 $\mu\text{Ci/ml}$ [^{14}C] cholesterol (American Radiolabeled Chemicals Inc, St. Louis, MO, USA). Cells were harvested by centrifugation, washed twice with synthetic complete (SC) media, diluted to an O.D.₆₀₀ of 1 into fresh SC media containing non-radiolabeled cholesterol and grown overnight. Cells were centrifuged and lipids were extracted from the cell pellet and the

culture supernatant using chloroform/methanol (v/v 1:1). Samples were dried and separated by thin-layer chromatography (TLC) using silica gel 60 plates (Merck, Darmstadt, Germany) using the solvent system, petroleum ether / diethyl ether /acetic acid (70:30:2; per vol.). Radiolabeled lipids on the TLC were quantified by scanning with a Berthold Tracemaster 40 Automatic TLC-Linear Analyzer (Berthold Technologies, Bad Wildbad, Germany). TLC plates were then exposed to phosphorimager screens and radiolabeled lipids were visualized using a phosphorimager (Bio-Rad Laboratories, Hercules, CA, USA).

2.8. In vitro sterol binding

In vitro sterol binding was assessed using a previously described radioligand-binding assay (Im et al., 2005; Choudhary and Schneiter, 2012; Darwiche and Schneiter, 2017). Briefly, 100 pmol of purified protein in binding buffer (20 mM Tris, pH 7.5, 30 mM NaCl, 0.05% Triton X-100) were incubated with 0–400 pmol of [³H]-cholesterol (American Radiolabeled Chemicals Inc., St Louis, Missouri, USA) for 1 h at 30 °C. The protein was adsorbed to Q-sepharose beads (GE healthcare) to remove unbound ligand, the beads were washed, and the radioligand was quantified by scintillation counting. For competition assays, 400 pmol of unlabeled cholesterol were included in the binding reaction, together with the indicated concentrations of [³H]-cholesterol. To determine non-specific binding, the ion exchange beads were incubated in the absence of added protein. At least two independent experiments were performed under each experimental condition and data are reported as the mean ± S.D. Calculation of the K_d value and curve fitting were performed using the statistical software Prism (GraphPad, La Jolla, CA, USA).

3. Results

3.1. Recombinant HpVAL-4

Expression of HpVAL-4 in our plant-based expression system resulted in a yield of 0.5–1.0 mg of pure recombinant protein per plant (3–4 g of leaf material). Recombinant HpVAL-4 was shown to be ~ 95% pure by a Coomassie stained SDS-PAGE gel (Fig. 1A). The oligomeric state of recombinant HpVAL-4 in solution was determined by measuring the absolute molecular mass by SEC-MALS. The protein gave a single peak on the sizing column (Fig. 1B) with a molecular mass of 21.07 ± 0.66 kDa, consistent with its theoretical molecular mass of 21.7 kDa, indicating that *HpVAL-4* forms a monomer in solution. It had been previously speculated that dimerization was important for the functions of SCP/TAPS proteins (Asojo et al., 2005; Gibbs et al., 2008). Our ongoing studies reveal that while some SCP/TAPS proteins such as MpPR-1i and SmVAL-4 form monomers in solution (Kelleher et al., 2015; Baroni et al., 2017), others including GAPR-1, Na-ASP-2 and GLIPR-1 form dimers in solution (Asojo et al., 2005; Gibbs et al., 2008).

The glycosylation composition of HpVAL-4 was then assessed by MALDI-TOF MS analysis of released N-glycans. All N-glycan types found on the HpVAL-4 protein carry typical plant beta(1,2)-xylose and core alpha(1,3)-fucose residues (Fig. 1C). Furthermore, the majority of the N-glycans are biantennary with terminal GlcNAc residues (GnGnXF³), but also paucimannosidic N-glycans (MMXF³) and N-glycans with one terminal GlcNAc residue were detected (MGnXF³ or GnMXF³). These latter structures likely arise from

apoplastic β -hexosaminidase activity (Shin et al., 2017). Altogether, our results demonstrate that plants are well suited as an expression platform for CAP proteins from helminths.

3.2. Crystal Structure of HpVAL-4

Each HpVAL-4 monomer folds as an alpha-beta-alpha sandwich, in which a beta sheet is sandwiched between two helical/loop regions (Fig. 2A). This classic SCP/TAPs motif is flanked by N-terminal and C-terminal extensions that are stabilized by disulfide bonds. While the refined model has four monomers of HpVAL-4 in the asymmetric unit (Supplementary Figs. S1, S2), this tetramer is likely an artifact of crystallization as SEC-MALS analysis indicates that HpVAL-4 is a monomer in solution. The monomers are very similar with root mean square deviation (rmsd) ranging between 0.075 Å to 0.176 Å for alignment of main chain atoms. The most variable regions between the monomers are loop regions, except the C-terminal extension that is virtually identical (Fig. 2B). The predicted N-linked glycosylation site Asn12 is glycosylated for all four monomers (Fig. 2A and B). The surface plot of HpVAL-4 reveals a large central CAP cavity of 1732.64 Å³, which is bordered by the first beta strand (β 1) and the third and fourth alpha helices (α 3, α 4), and opens into a C-terminal loop (Fig. 2). This cavity is comparable in size to previously reported SCP/TAPs protein structures (Asojo et al., 2005, 2011; Gibbs et al., 2008; Wang et al., 2010a; Asojo, 2011; Ma et al., 2011; Kelleher et al., 2015). Additionally, within the crystallographic tetramer there are no possible dimers that have packing similar to either the two-CAP Na-ASP-1 or the dimer in Pry1 that connect both central CAP cavities (Asojo, 2011; Darwiche et al., 2016).

3.4. HpVAL-4 rescues the cholesterol export defect in *pry1 pry2* mutant cells and binds sterol in vitro

To test whether expression of HpVAL-4 in *pry1 pry2* mutant cells rescued the defect in cholesterol export, heme-deficient cells containing either an empty plasmid or a plasmid with HpVAL-4 were radiolabeled with [¹⁴C]cholesterol overnight, washed and diluted in fresh media to allow for export of cholesterol and cholesteryl acetate. Lipids were extracted from the cell pellet (P) and the culture supernatant (S), and separated by thin layer chromatography (Fig. 3A). The levels of free cholesterol and cholesteryl acetate were quantified by radio scanning and the relative percentages of cholesteryl acetate exported by the cells were plotted as the export index which is the ratio between the extracellular cholesteryl acetate and the sum of intra- and extra-cellular cholesteryl acetate (Fig. 3B). Cells complemented with HpVAL-4 exported cholesteryl acetate into the culture supernatant at levels comparable to wild-type cells and Pry1 indicating that HpVAL-4 is an effective exporter.

HpVAL-4 was determined to bind cholesterol in vitro, by a direct binding assay in which increasing concentrations of [³H]-cholesterol (0–400 pmol) were incubated with 100 pmol of HpVAL-4 proteins. The protein was separated from unbound ligand by adsorption to an anion-exchange matrix and bound radioligand was quantified by scintillation counting. HpVAL-4 binds cholesterol in vitro with a saturable k_d of 1.53 μ M, which is comparable to that of Pry1 (k_d of 1.25 μ M) (Darwiche et al., 2016). Furthermore, cholesterol binding is specific as addition of unlabeled cholesterol (400 pmol) competes with radioligand binding

(Fig. 3C). These binding studies show that HpVAL-4 binds [³H]-cholesterol in a concentration-dependent manner and that binding of the radiolabeled ligand can be competed with by incubation with unlabeled cholesterol (Fig. 3C).

4. Discussion

Using structural similarity in PDBeFold (<http://www.ebi.ac.uk/msd-srv/ssm/>), a three-dimensional (3-D) structural alignment that takes both the alignment length and rmsd into account, structures that were most similar to HpVAL-4 were identified as CAP proteins that have less than 30% sequence identity with HpVAL-4. The most similar structure to HpVAL-4 is that of Na-ASP-2, (Asojo et al., 2005; Mason et al., 2014) followed by human hookworm platelet inhibitor, HPI (Ma et al., 2015), *Ancylostoma*-secreted protein, Ac-ASP-7 (Osman et al., 2012), *Schistosoma mansoni* venom allergen-like protein 4, SmVAL4, (Kelleher et al., 2015), tablysin-15 (Ma et al., 2011), pry1 (Darwiche et al., 2016), human GAPR-1 (van Galen et al., 2012) and P14A from tomato (Fernandez et al., 1997). HpVAL-4 shares a conserved C-terminal extension with Na-ASP-2 that has two strands, which are stabilized by two disulfide bonds. This C-terminal extension is more varied in HPI, SmVAL4 and Ac-ASP-7. The flexible N-terminal loops of both proteins also have a conserved disulfide bond with alpha helix 2.

Only two proteins with greater than 30% sequence identity with HpVAL-4 have reported crystal structures, *Necator americanus* ASP-1 (Asojo, 2011) and *Ostertagia ostertagi* ASP-1 (Borloo et al., 2013). Neither was a top hit based on PDBeFold analysis due to the variations in the loop regions that make up over 45% of the topology of CAP proteins. Interestingly, reverse template alignment using ProFunc (Laskowski et al., 2005; Laskowski, 2017) reveals that both structures are certain matches (E-value < 1.00E-06) and while there are indeed insertions and gaps in loop regions, the topology of many of the helices and strands are conserved (Supplementary Figs. S3, S4). As previously mentioned, the loop regions are flexible and varied for SCP/TAPS protein structures and make it difficult to model the structures. Furthermore, even among those that share structural similarity with HpVAL-4, the lengths of loops differ (Fig. 4).

Despite the difference in the orientation of its loop region, HpVAL-4 has a central exposed cavity similar to previously reported SCP/TAPS protein structures (Asojo et al., 2005., 2011; Gibbs et al., 2008; Asojo, 2011). Since HpVAL-4 lacks the histidines that bind divalent cations, it is unable to coordinate Zn²⁺ for the proposed heparin-sulfate-dependent mechanisms of inflammatory modulation by the cobra CRISP natrin (Wang et al., 2010a). The sequence of amino acid residues in the CAP cavity of HpVAL-4 is more similar to that of the N-terminal CAP domain of Na-ASP-1 (Fig. 4, Supplementary Fig. S4). Comparison of the CAP cavity suggests that HpVAL-4 and the N-terminal CAP domain of Na-ASP-1 may present a different motif for hookworms and more studies are needed to identify the biological relevance of the conserved residues.

It was previously shown that *Saccharomyces cerevisiae* CAP proteins are required for cholesteryl acetate transport (Choudhary and Schneiter, 2012; Choudhary et al., 2014) and we now report that HpVAL-4 rescues the sterol-binding function of yeast that lacked the

endogenous CAP proteins Pry1 and Pry2, and that recombinant HpVAL-4 binds sterol in vitro (Fig. 3). While HpVAL-4 has less than 30% sequence similarity to Pry1 and Pry2, it also shares limited structural similarity with Pry1 (Fig. 4). It has been shown that a caveolin-binding motif (CBM), which is located in a flexible loop region connecting helices $\alpha 3$ and $\alpha 4$ (Figs. 2, 4), that has several polar amino acid residues capable of interacting with lipids, is important for both in vivo and in vitro sterol binding by Pry1 (Choudhary et al., 2014). The amino acid sequence of the CBM is characterized by the presence of conserved aromatic amino acids, which are required for the in vivo export and the in vitro binding of sterols in SCP/TAPS proteins. The CBM loop of HpVAL-4 has a different conformation from Pry1 but creates a cavity that is large enough to accommodate dioxane, as was observed in the structure of Pry1 (Fig. 5). Interestingly, the insertion of a string of glutamic acid residues makes the cavity less hydrophobic than observed for Pry1 (Fig. 4). Our analysis shows that HpVAL-4 has comparable in vitro cholesterol binding ability to Pry1 (Fig. 3C).

A second distinct and independent lipid-binding function of SCP/TAPS proteins is the palmitate binding observed in a cavity between two helices as observed in tabylsin-15. This cavity was also shown to bind leukotriene (Xu et al., 2012). The locations of alpha helices 1 and 4 are conserved in SCP/TAPS proteins including HpVAL-4 (Figs. 2, 4). As previously indicated for other CAP proteins, the amino acid residues in the palmitate binding cavity are poorly conserved, however there is sufficient space between the equivalent helices to facilitate palmitate binding (Figs. 2, 6). These analyses reveal that HpVAL-4 is structurally able to bind palmitate, as was observed for tabylsin-15. This suggests that HpVAL4 may be able to bind other fatty acids and fatty acid-derived products such as the immunologically relevant prostaglandins and leukotrienes. Such a role in immune modulation, rather than lipid transport within the *H. polygyrus* organism, is also indicated by its expression across all mammalian stages of the parasite, and its prominent secretion by both tissue-stage larvae and luminal-dwelling adults of the species (Hewitson et al., 2013). Further studies will shed light on whether HpVAL-4 indeed has such an immunomodulatory function.

Hp-VAL-4 produced in our plant expression system is a glycosylated protein that readily crystallized from high concentrations of PEG. HpVAL-4 is a monomer in solution and retains a large open palmitate-binding cavity, making it capable of binding this and other lipids. Additionally, the presence of a large CBM explains the ability of HpVAL-4 to export sterol in vivo. HpVAL-4 has a large central cavity that lacks the prototypical CAP cavity tetrad, which means it will be incapable of binding divalent cations. The amino acid residues in the CAP cavity of HpVAL-4 are more similar to those in the amino terminal CAP domain of the two CAP Na-ASP-1. Studies are underway to determine endogenous binding partners of HpVAL-4 and other SCP/TAP proteins from parasites.

Supplementary Material

Refer to Web version on PubMed Central for supplementary material.

Acknowledgments

Thanks to Prof. Cornelis H. Hokke and Ms D. Linh Nguyen from Leiden University Medical Center, Netherlands, for N-glycan structure analysis, Dr. Sukyeong Lee of the Biochemistry Department, Baylor College of Medicine, USA, for access to the X-ray facility, and Dr. Mitchell Miller of Rice University, USA, for screening for diffraction of initial crystals. OAA was supported by startup funds from the National School of Tropical Medicine, Baylor College of Medicine. Funders for these studies include the Netherlands Organization for Scientific Research (ALW 84713008), and the Swiss National Science Foundation (31003A_153416 to RS). SG was funded by US National Institute of Health minority diversity initiative to maximize research education in genomics, (R25-HG006674-02). RMM and CD were supported by both a Wellcome Trust UK investigator award (Ref 106122), and Wellcome Trust core funding to the Wellcome Centre for Molecular Parasitology UK (Ref 104111).

References

- Adams PD, Afonine PV, Bunkoczi G, Chen VB, Davis IW, Echols N, Headd JJ, Hung LW, Kapral GJ, Grosse-Kunstleve RW, McCoy AJ, Moriarty NW, Oeffner R, Read RJ, Richardson DC, Richardson JS, Terwilliger TC, Zwart PH. PHENIX: a comprehensive Python-based system for macromolecular structure solution. *Acta Cryst D*. 2010; 66:213–221. [PubMed: 20124702]
- Asojo OA. Structure of a two-CAP-domain protein from the human hookworm parasite *Necator americanus*. *Acta Cryst D*. 2011; 67:455–462. [PubMed: 21543848]
- Asojo OA, Goud G, Dhar K, Loukas A, Zhan B, Deumic V, Liu S, Borgstahl GE, Hotez PJ. X-ray structure of Na-ASP-2, a pathogenesis-related-1 protein from the nematode parasite, *Necator americanus*, and a vaccine antigen for human hookworm infection. *J Mol Biol*. 2005; 346:801–814. [PubMed: 15713464]
- Asojo OA, Koski RA, Bonafe N. Structural studies of human glioma pathogenesis-related protein 1. *Acta Cryst D*. 2011; 67:847–855. [PubMed: 21931216]
- Baroni RM, Luo Z, Darwiche R, Hudspeth EM, Schneiter R, Pereira GAG, Mondego JMC, Asojo OA. Crystal Structure of MpPR-1i, a SCP/TAPS protein from *Moniliophthora perniciosa*, the fungus that causes Witches' Broom Disease of Cacao. *Sci Rep*. 2017; 7:7818. [PubMed: 28798297]
- Behnke JM. Evasion of immunity by nematode parasites causing chronic infections. *Adv Parasitol*. 1987; 26:1–71. [PubMed: 3314404]
- Behnke JM, Menge DM, Noyes H. *Heligmosomoides bakeri*: a model for exploring the biology and genetics of resistance to chronic gastrointestinal nematode infections. *Parasitology*. 2009; 136:1565–1580. [PubMed: 19450375]
- Bethony J, Loukas A, Smout M, Brooker S, Mendez S, Plieskatt J, Goud G, Bottazzi ME, Zhan B, Wang Y, Williamson A, Lustigman S, Correa-Oliveira R, Xiao S, Hotez PJ. Antibodies against a secreted protein from hookworm larvae reduce the intensity of hookworm infection in humans and vaccinated laboratory animals. *Faseb J*. 2005; 19:1743–1745. [PubMed: 16037096]
- Borloo J, Geldhof P, Peelaers I, Van Meulder F, Ameloot P, Callewaert N, Vercruyse J, Claerebout E, Strelkov SV, Weeks SD. Structure of *Ostertagia ostertagi* ASP-1: insights into disulfide-mediated cyclization and dimerization. *Acta Cryst D*. 2013; 69:493–503. [PubMed: 23519657]
- Cantacessi C, Campbell BE, Visser A, Geldhof P, Nolan MJ, Nisbet AJ, Matthews JB, Loukas A, Hofmann A, Otranto D, Sternberg PW, Gasser RB. A portrait of the “SCP/TAPS” proteins of eukaryotes—developing a framework for fundamental research and biotechnological outcomes. *Biotechnol Adv*. 2009; 27:376–388. [PubMed: 19239923]
- Cantacessi C, Mitreva M, Jex AR, Young ND, Campbell BE, Hall RS, Doyle MA, Ralph SA, Rabelo EM, Ranganathan S, Sternberg PW, Loukas A, Gasser RB. Massively parallel sequencing and analysis of the *Necator americanus* transcriptome. *PLoS Negl Trop Dis*. 2010; 4:e684. [PubMed: 20485481]
- Choudhary V, Darwiche R, Gfeller D, Zoete V, Michielin O, Schneiter R. The caveolin-binding motif of the pathogen-related yeast protein Pry1, a member of the CAP protein superfamily, is required for in vivo export of cholesteryl acetate. *J Lipid Res*. 2014; 55:883–894. [PubMed: 24598142]
- Choudhary V, Schneiter R. Pathogen-Related Yeast (PRY) proteins and members of the CAP superfamily are secreted sterol-binding proteins. *Proc Natl Acad Sci USA*. 2012; 109:16882–16887.

- Darwiche R, Kelleher A, Hudspeth EM, Schneider R, Asojo OA. Structural and functional characterization of the CAP domain of pathogen-related yeast 1 (Pry1) protein. *Sci Rep.* 2016; 6:28838. [PubMed: 27344972]
- Darwiche R, Schneider R. A Ligand-Binding Assay to Measure the Affinity and Specificity of Sterol-Binding Proteins In Vitro. *Methods Mol Biol.* 2017; 1645:361–368. [PubMed: 28710641]
- Ding X, Shields J, Allen R, Hussey RS. Molecular cloning and characterisation of a venom allergen AG5-like cDNA from *Meloidogyne incognita*. *Int J Parasitol.* 2000; 30:77–81. [PubMed: 10675748]
- Emsley P, Lohkamp B, Scott WG, Cowtan K. Features and development of Coot. *Acta Cryst D.* 2010; 66:486–501. [PubMed: 20383002]
- Fernandez C, Szyperski T, Bruyere T, Ramage P, Mosinger E, Wuthrich K. NMR solution structure of the pathogenesis-related protein P14a. *J Mol Biol.* 1997; 266:576–593. [PubMed: 9067611]
- Ferreira I, Smyth D, Gaze S, Aziz A, Giacomini P, Ruysers N, Artis D, Laha T, Navarro S, Loukas A, McSorley HJ. Hookworm excretory/secretory products induce interleukin-4 (IL-4)+ IL-10+ CD4+ T cell responses and suppress pathology in a mouse model of colitis. *Infect Immun.* 2013; 81:2104–2111. [PubMed: 23545299]
- Finney CA, Taylor MD, Wilson MS, Maizels RM. Expansion and activation of CD4(+)CD25(+) regulatory T cells in *Heligmosomoides polygyrus* infection. *Eur J Immunol.* 2007; 37:1874–1886. [PubMed: 17563918]
- Fujiwara RT, Bethony J, Bueno LL, Wang Y, Ahn SY, Samuel A, Bottazzi ME, Hotez P, Mendez S. Immunogenicity of the hookworm Na-ASP-2 vaccine candidate: characterization of humoral and cellular responses after vaccination in the Sprague Dawley rat. *Hum Vaccin.* 2005; 1:123–128. [PubMed: 17012856]
- Gao B, Allen R, Maier T, Davis EL, Baum TJ, Hussey RS. Molecular characterisation and expression of two venom allergen-like protein genes in *Heterodera glycines*. *Int J Parasitol.* 2001; 31:1617–1625. [PubMed: 11730789]
- Gibbs GM, O'Bryan MK. Cysteine rich secretory proteins in reproduction and venom. *Soc Reprod Fertil Suppl.* 2007; 65:261–267. [PubMed: 17644967]
- Gibbs GM, Roelants K, O'Bryan MK. The CAP superfamily: cysteine-rich secretory proteins, antigen 5, and pathogenesis-related 1 proteins—roles in reproduction, cancer, and immune defense. *Endocr Rev.* 2008; 29:865–897. [PubMed: 18824526]
- Gonzalez-Hernandez A, Van Coppennolle S, Borloo J, Van Meulder F, Paerewijck O, Peelaers I, Leclercq G, Claerebout E, Geldhof P. Host protective ASP-based vaccine against the parasitic nematode *Ostertagia ostertagi* triggers NK cell activation and mixed IgG1-IgG2 response. *Sci Rep.* 2016; 6:29496. [PubMed: 27403891]
- Gouet P, Robert X, Courcelle E. ESPript/ENDscript: Extracting and rendering sequence and 3D information from atomic structures of proteins. *Nucleic Acids Res.* 2003; 31:3320–3323. [PubMed: 12824317]
- Guo M, Teng M, Niu L, Liu Q, Huang Q, Hao Q. Crystal structure of the cysteine-rich secretory protein stecrisp reveals that the cysteine-rich domain has a K⁺ channel inhibitor-like fold. *J Biol Chem.* 2005; 280:12405–12412. [PubMed: 15596436]
- Harris NL, Pleass R, Behnke JM. Understanding the role of antibodies in murine infections with *Heligmosomoides (polygyrus) bakeri*: 35 years ago, now and 35 years ahead. *Parasite Immunol.* 2014; 36:115–124. [PubMed: 23889357]
- Hawdon JM, Narasimhan S, Hotez PJ. *Ancylostoma* secreted protein 2: cloning and characterization of a second member of a family of nematode secreted proteins from *Ancylostoma caninum*. *Mol Biochem Parasitol.* 1999; 99:149–165. [PubMed: 10340481]
- He Y, Barker SJ, MacDonald AJ, Yu Y, Cao L, Li J, Parhar R, Heck S, Hartmann S, Golenbock DT, Jiang S, Libri NA, Semper AE, Rosenberg WM, Lustigman S. Recombinant Ov-ASP-1, a Th1-biased protein adjuvant derived from the helminth *Onchocerca volvulus*, can directly bind and activate antigen-presenting cells. *J Immunol.* 2009; 182:4005–4016. [PubMed: 19299698]
- Hewitson JP, Filbey KJ, Grainger JR, Dowle AA, Pearson M, Murray J, Harcus Y, Maizels RM. *Heligmosomoides polygyrus* elicits a dominant nonprotective antibody response directed against restricted glycan and peptide epitopes. *J Immunol.* 2011a; 187:4764–4777. [PubMed: 21964031]

- Hewitson JP, Grainger JR, Maizels RM. Helminth immunoregulation: the role of parasite secreted proteins in modulating host immunity. *Mol Biochem Parasitol.* 2009; 167:1–11. [PubMed: 19406170]
- Hewitson JP, Harcus Y, Murray J, van Agtmaal M, Filbey KJ, Grainger JR, Bridgett S, Blaxter ML, Ashton PD, Ashford DA, Curwen RS, Wilson RA, Dowle AA, Maizels RM. Proteomic analysis of secretory products from the model gastrointestinal nematode *Heligmosomoides polygyrus* reveals dominance of venom allergen-like (VAL) proteins. *J Proteomics.* 2011b; 74:1573–1594. [PubMed: 21722761]
- Hewitson JP, Ivens AC, Harcus Y, Filbey KJ, McSorley HJ, Murray J, Bridgett S, Ashford D, Dowle AA, Maizels RM. Secretion of protective antigens by tissue-stage nematode larvae revealed by proteomic analysis and vaccination-induced sterile immunity. *PLoS Pathog.* 2013; 9:e1003492. [PubMed: 23966853]
- Im YJ, Raychaudhuri S, Prinz WA, Hurley JH. Structural mechanism for sterol sensing and transport by OSBP-related proteins. *Nature.* 2005; 437:154–158. [PubMed: 16136145]
- Johnston MJ, MacDonald JA, McKay DM. Parasitic helminths: a pharmacopeia of anti-inflammatory molecules. *Parasitology.* 2009; 136:125–147. [PubMed: 19079844]
- Kelleher A, Darwiche R, Rezende WC, Farias LP, Leite LC, Schneiter R, Asojo OA. *Schistosoma mansoni* venom allergen-like protein 4 (SmVAL4) is a novel lipid-binding SCP/TAPS protein that lacks the prototypical CAP motifs. *Acta Cryst D.* 2015; 70:2186–96.
- Laskowski RA. The ProFunc Function Prediction Server. *Methods Mol Biol.* 2017; 1611:75–95. [PubMed: 28451973]
- Laskowski RA, Watson JD, Thornton JM. ProFunc: a server for predicting protein function from 3D structure. *Nucleic Acids Res.* 2005; 33:W89–93. [PubMed: 15980588]
- Leslie AG. The integration of macromolecular diffraction data. *Acta Cryst D.* 2006; 62:48–57. [PubMed: 16369093]
- Ma D, Francischetti IM, Ribeiro JM, Andersen JF. The structure of hookworm platelet inhibitor (HPI), a CAP superfamily member from *Ancylostoma caninum*. *Acta Cryst F.* 2015; 71:643–649.
- Ma D, Xu X, An S, Liu H, Yang X, Andersen JF, Wang Y, Tokumasu F, Ribeiro JM, Francischetti IM, Lai R. A novel family of RGD-containing disintegrins (Tablysin-15) from the salivary gland of the horsefly *Tabanus yao* targets alphaIIb beta3 or alphaV beta3 and inhibits platelet aggregation and angiogenesis. *Thromb Haemost.* 2011; 105:1032–1045. [PubMed: 21475772]
- Mason L, Tribolet L, Simon A, von Gnielinski N, Nienaber L, Taylor P, Willis C, Jones MK, Sternberg PW, Gasser RB, Loukas A, Hofmann A. Probing the equatorial groove of the hookworm protein and vaccine candidate antigen, Na-ASP-2. *Int J Biochem Cell Biol.* 2014; 50:146–155. [PubMed: 24631931]
- McCoy AJ, Grosse-Kunstleve RW, Storoni LC, Read RJ. Likelihood-enhanced fast translation functions. *Acta Cryst D.* 2005; 61:458–464. [PubMed: 15805601]
- Morris RJ, Perrakis A, Lamzin VS. ARP/wARP and automatic interpretation of protein electron density maps. *Methods Enzymol.* 2003; 374:229–244. [PubMed: 14696376]
- Morris RJ, Zwart PH, Cohen S, Fernandez FJ, Kakaris M, Kirillova O, Vornrhein C, Perrakis A, Lamzin VS. Breaking good resolutions with ARP/wARP. *J Synchrotron Radiat.* 2004; 11:56–59. [PubMed: 14646134]
- Murshudov GN, Skubak P, Lebedev AA, Pannu NS, Steiner RA, Nicholls RA, Winn MD, Long F, Vagin AA. REFMAC5 for the refinement of macromolecular crystal structures. *Acta Cryst D.* 2011; 67:355–367. [PubMed: 21460454]
- Osman A, Wang CK, Winter A, Loukas A, Tribolet L, Gasser RB, Hofmann A. Hookworm SCP/TAPS protein structure – A key to understanding host-parasite interactions and developing new interventions. *Biotechnol Adv.* 2012; 30:652–657. [PubMed: 22120067]
- Pflugrath JW. The finer things in X-ray diffraction data collection. *Acta Cryst D.* 1999; 55(Pt 10): 1718–1725. [PubMed: 10531521]
- Rausch S, Huehn J, Kirchhoff D, Rzepecka J, Schnoeller C, Pillai S, Loddenkemper C, Scheffold A, Hamann A, Lucius R, Hartmann S. Functional analysis of effector and regulatory T cells in a parasitic nematode infection. *Infect Immun.* 2008; 76:1908–1919. [PubMed: 18316386]

- Reynolds LA, Filbey KJ, Maizels RM. Immunity to the model intestinal helminth parasite *Heligmosomoides polygyrus*. *Semin Immunopathol.* 2012; 34:829–846. [PubMed: 23053394]
- Robinson M, Wahid F, Behnke JM, Gilbert FS. Immunological relationships during primary infection with *Heligmosomoides polygyrus* (*Nematospiroides dubius*): dose-dependent expulsion of adult worms. *Parasitology.* 1989; 98(Pt 1):115–124. [PubMed: 2717211]
- Serrano RL, Kuhn A, Hendricks A, Helms JB, Sinning I, Groves MR. Structural analysis of the human Golgi-associated plant pathogenesis related protein GAPR-1 implicates dimerization as a regulatory mechanism. *J Mol Biol.* 2004; 339:173–183. [PubMed: 15123429]
- Shikamoto Y, Suto K, Yamazaki Y, Morita T, Mizuno H. Crystal structure of a CRISP family Ca²⁺ - channel blocker derived from snake venom. *J Mol Biol.* 2005; 350:735–743. [PubMed: 15953617]
- Shin YJ, Castilho A, Dicker M, Sadio F, Vavra U, Grunwald-Gruber C, Kwon TH, Altmann F, Steinkellner H, Strasser R. Reduced paucimannosidic N-glycan formation by suppression of a specific beta-hexosaminidase from *Nicotiana benthamiana*. *Plant Biotechnol J.* 2017; 15:197–206. [PubMed: 27421111]
- Smith KA, Filbey KJ, Reynolds LA, Hewitson JP, Marcus Y, Boon L, Sparwasser T, Hammerling G, Maizels RM. Low-level regulatory T-cell activity is essential for functional type-2 effector immunity to expel gastrointestinal helminths. *Mucosal Immunol.* 2016; 9:428–443. [PubMed: 26286232]
- Storoni LC, McCoy AJ, Read RJ. Likelihood-enhanced fast rotation functions. *Acta Cryst D.* 2004; 60:432–438. [PubMed: 14993666]
- Suzuki N, Yamazaki Y, Brown RL, Fujimoto Z, Morita T, Mizuno H. Structures of pseudochetoxin and pseudodecin, two snake-venom cysteine-rich secretory proteins that target cyclic nucleotide-gated ion channels: implications for movement of the C-terminal cysteine-rich domain. *Acta Cryst D.* 2008; 64:1034–1042. [PubMed: 18931410]
- Svetic A, Madden KB, Zhou XD, Lu P, Katona IM, Finkelman FD, Urban JF Jr, Gause WC. A primary intestinal helminthic infection rapidly induces a gut-associated elevation of Th2-associated cytokines and IL-3. *J Immunol.* 1993; 150:3434–3441. [PubMed: 8468481]
- Terwilliger TC, Grosse-Kunstleve RW, Afonine PV, Moriarty NW, Zwart PH, Hung LW, Read RJ, Adams PD. Iterative model building, structure refinement and density modification with the PHENIX AutoBuild wizard. *Acta Cryst D.* 2008; 64:61–69. [PubMed: 18094468]
- Tiwari R, Koffel R, Schneider R. An acetylation/deacetylation cycle controls the export of sterols and steroids from *S. cerevisiae*. *EMBO J.* 2007; 26:5109–5119. [PubMed: 18034159]
- van Galen J, Orlachs NK, Schouten A, Serrano RL, Nolte-t Hoen EN, Eerland R, Kaloyanova D, Gros P, Helms JB. Interaction of GAPR-1 with lipid bilayers is regulated by alternative homodimerization. *Biochim Biophys Acta.* 2012; 1818:2175–2183. [PubMed: 22560898]
- Van Galen J, Van Balkom BW, Serrano RL, Kaloyanova D, Eerland R, Stuken E, Helms JB. Binding of GAPR-1 to negatively charged phospholipid membranes: unusual binding characteristics to phosphatidylinositol. *Mol Membr Biol.* 2010; 27:81–91. [PubMed: 20095951]
- Vervovski-Almeida S, DeMarco R, Martins EA, Guimaraes PE, Ojopi EP, Paquola AC, Piazza JP, Nishiyama MY Jr, Kitajima JP, Adamson RE, Ashton PD, Bonaldo MF, Coulson PS, Dillon GP, Farias LP, Gregorio SP, Ho PL, Leite RA, Malaquias LC, Marques RC, Miyasato PA, Nascimento AL, Ohlweiler FP, Reis EM, Ribeiro MA, Sa RG, Stukart GC, Soares MB, Gargioni C, Kawano T, Rodrigues V, Madeira AM, Wilson RA, Menck CF, Setubal JC, Leite LC, Dias-Neto E. Transcriptome analysis of the acelomate human parasite *Schistosoma mansoni*. *Nat Genet.* 2003; 35:148–157. [PubMed: 12973350]
- Wahid FN, Behnke JM, Grecis RK, Else KJ, Ben-Smith AW. Immunological relationships during primary infection with *Heligmosomoides polygyrus*: Th2 cytokines and primary response phenotype. *Parasitology.* 1994; 108(Pt 4):461–471. [PubMed: 8008460]
- Wang J, Shen B, Guo M, Lou X, Duan Y, Cheng XP, Teng M, Niu L, Liu Q, Huang Q, Hao Q. Blocking effect and crystal structure of natriin toxin, a cysteine-rich secretory protein from *Naja atra* venom that targets the BKCa channel. *Biochemistry.* 2005; 44:10145–10152. [PubMed: 16042391]
- Wang YL, Kuo JH, Lee SC, Liu JS, Hsieh YC, Shih YT, Chen CJ, Chiu JJ, Wu WG. Cobra CRISP Functions as an Inflammatory Modulator via a Novel Zn²⁺- and Heparan Sulfate-dependent

- Transcriptional Regulation of Endothelial Cell Adhesion Molecules. *J Biol Chem.* 2010a; 285:37872–37883. [PubMed: 20889969]
- Wang Z, Abubucker S, Martin J, Wilson RK, Hawdon J, Mitreva M. Characterizing *Ancylostoma caninum* transcriptome and exploring nematode parasitic adaptation. *BMC Genomics.* 2010b; 11:307. [PubMed: 20470405]
- Wilbers RH, Westerhof LB, van Noort K, Obieglo K, Driessen NN, Everts B, Gringhuis SI, Schramm G, Goverse A, Smant G, Bakker J, Smits HH, Yazdanbakhsh M, Schots A, Hokke CH. Production and glyco-engineering of immunomodulatory helminth glycoproteins in plants. *Sci Rep.* 2017; 7:45910. [PubMed: 28393916]
- Winn MD, Ballard CC, Cowtan KD, Dodson EJ, Emsley P, Evans PR, Keegan RM, Krissinel EB, Leslie AG, McCoy A, McNicholas SJ, Murshudov GN, Pannu NS, Potterton EA, Powell HR, Read RJ, Vagin A, Wilson KS. Overview of the CCP4 suite and current developments. *Acta Cryst D.* 2011; 67:235–242. [PubMed: 21460441]
- Xu X, Francischetti IM, Lai R, Ribeiro JM, Andersen JF. Structure of protein having inhibitory disintegrin and leukotriene scavenging functions contained in single domain. *J Biol Chem.* 2012; 287:10967–10976. [PubMed: 22311975]
- Zhan B, Liu Y, Badamchian M, Williamson A, Feng J, Loukas A, Hawdon JM, Hotez PJ. Molecular characterisation of the *Ancylostoma*-secreted protein family from the adult stage of *Ancylostoma caninum*. *Int J Parasitol.* 2003; 33:897–907. [PubMed: 12906874]

Highlights

- *Heligmosomoides polygyrus* Venom Allergen-like Protein-4 (HpVAL-4) was produced in plants as a glycosylated protein.
- The crystal structure of HpVAL-4 was solved and reveals three distinct cavities.
- These cavities are the central cavity; the sterol-binding caveolin-binding motif (CBM); and the palmitate-binding cavity.
- The central cavity of Hp-VAL-4 lacks the characteristic histidines that coordinate divalent cations
- Hp-VAL-4 binds sterol in vivo and in vitro]

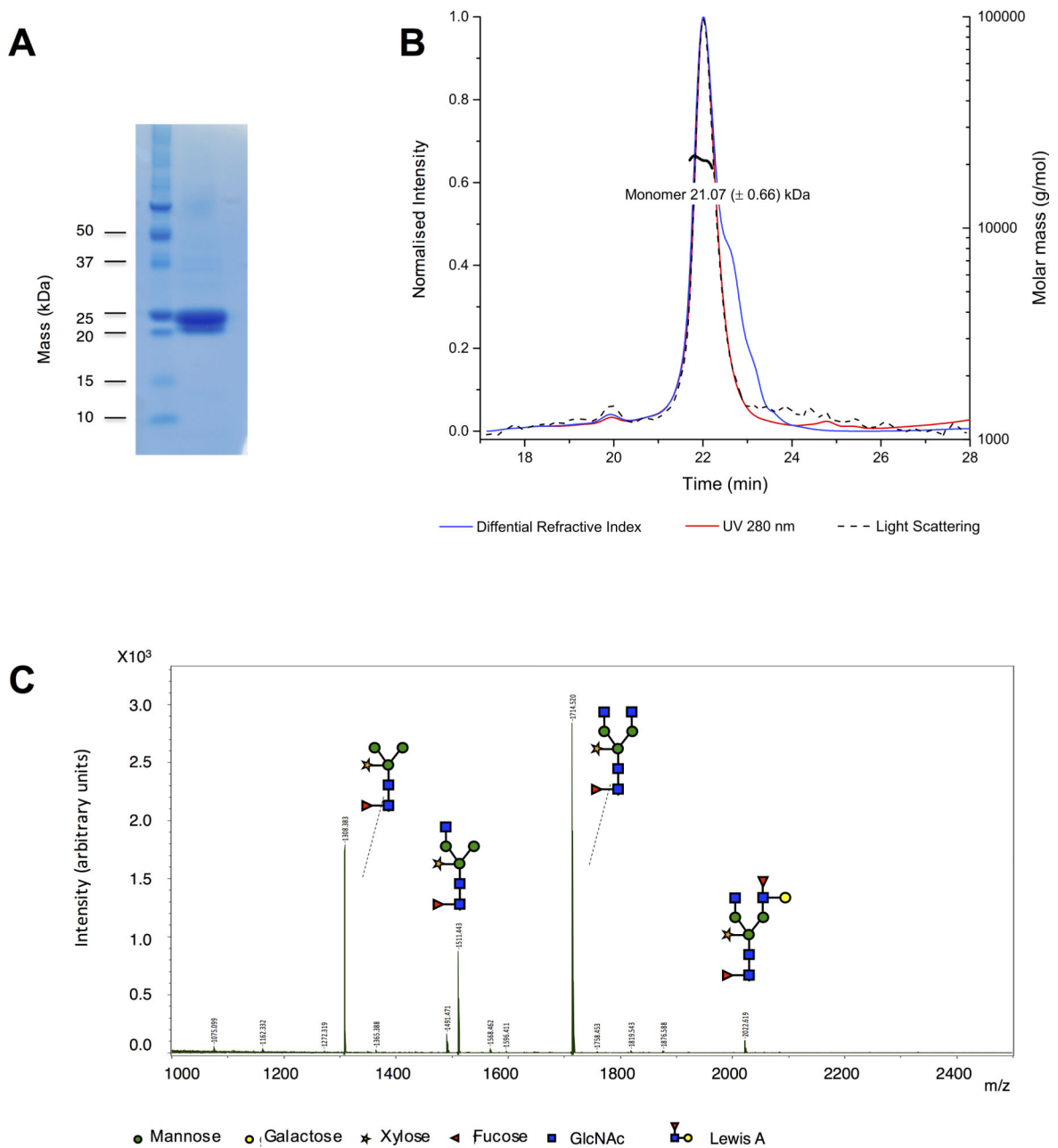


Fig. 1. Protein purity and characterization of *Heligmosomoides polygyrus* Venom Allergen-like Protein-4 (HpVAL-4). (A) Coomassie-stained SDS gel reveals the purity of recombinant HpVAL-4 and its monomeric mass of ~22 kDa. (B) Size exclusion chromatography multi-angle light scattering (SEC-MALS) analysis reveals that HpVAL-4 is an ~ 21 kDa monomer in solution. (C) N-glycan composition of plant-produced HpVAL-4.

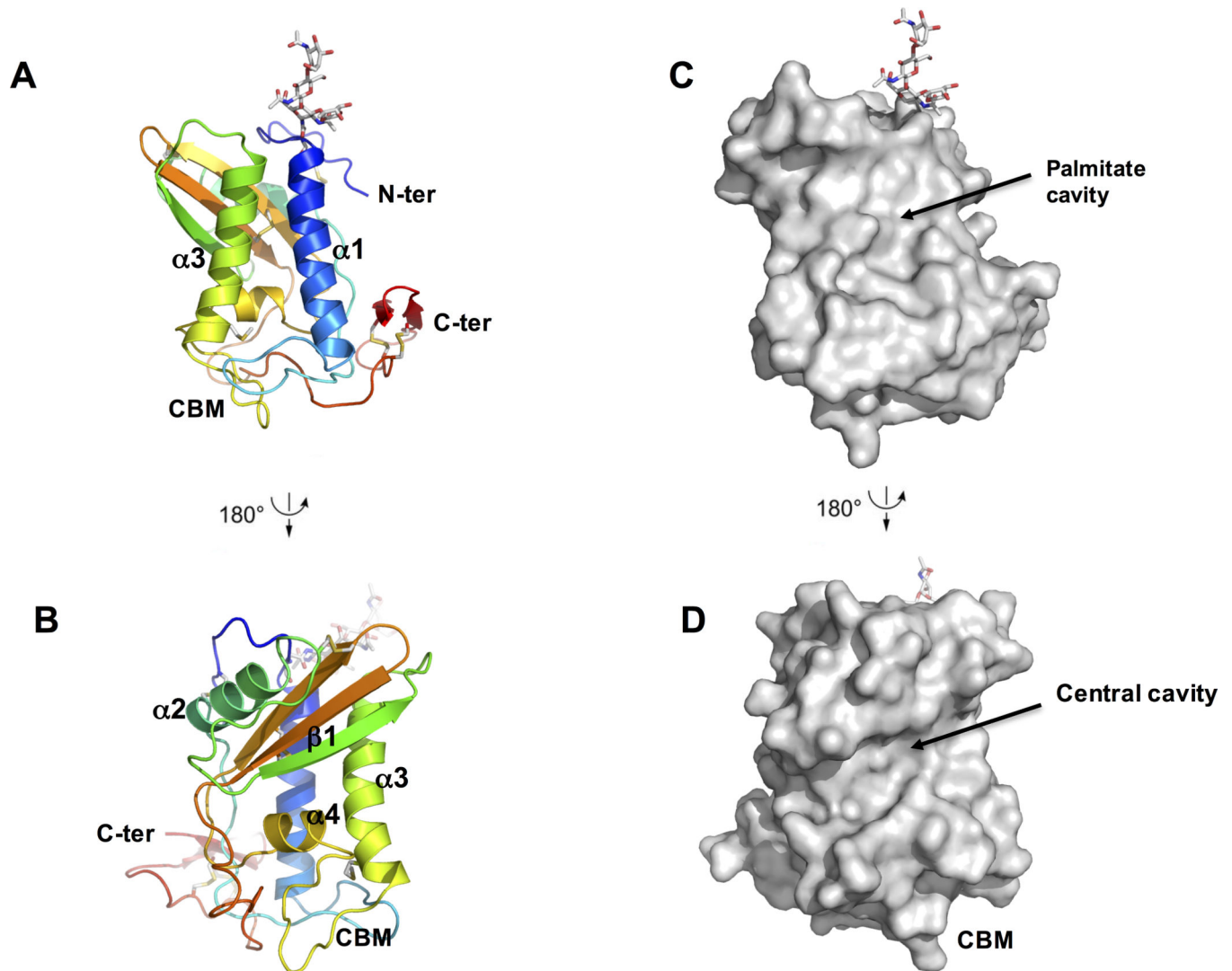


Fig. 2. Crystal structure of *Heligmosomoides polygyrus* Venom Allergen-like Protein-4 (HpVAL-4). (A) Cartoon of a monomer of HpVAL-4 rainbow colours from amino (blue) to carboxyl terminus (red). The two longest helices $\alpha 1$ and $\alpha 3$ that form the palmitate cavity and the calveolin binding motif loop (CBM) are indicated, while glycans and disulfide bridges are shown in stick form (colored by elements: blue for N, white for C, red for O, and yellow for S). (B) Rotation (180 degrees) of the monomer allows better visualization of the strand ($\beta 1$) and helix ($\alpha 4$) that form the central cavity. (C, D) Surface representations of the views for A and B, respectively.

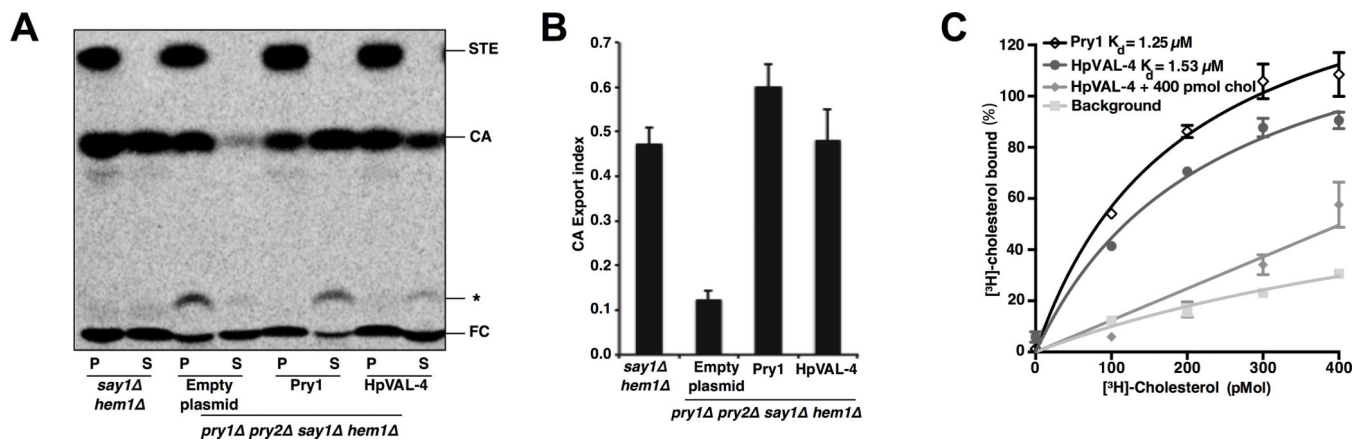


Fig. 3.

Heligmosomoides polygyrus Venom Allergen-like Protein-4 (HpVAL-4) exports and binds cholesterol in vivo and in vitro. (A) Expression of HpVAL-4 complements the sterol export defect of yeast cells lacking their endogenous cysteine-rich secretory proteins, antigen 5, and pathogenesis-related 1 (CAP) proteins (Pry1 and Pry2). Heme-deficient cells of the indicated genotype containing either an empty plasmid or a plasmid with Pry1 or HpVAL-4 were radiolabeled with [¹⁴C]cholesterol overnight, washed and diluted in fresh media to allow for export of cholesterol and cholesteryl acetate. Lipids were extracted from the cell pellet (P) and the culture supernatant (S), and separated by thin layer chromatography. The positions of free cholesterol (FC), cholesteryl acetate (CA) and sterol esters (STE) are indicated. The star marks the position of an unidentified cholesterol derivative. (B) Quantification of the export of cholesteryl acetate in yeast cells lacking their endogenous CAP proteins when complemented with empty plasmid, Pry1 or HpVAL-4. The export index indicates the relative percentages of cholesteryl acetate that is exported by the cells (ratio between the extracellular cholesteryl acetate and the sum of intra- and extra-cellular cholesteryl acetate). Data represent mean \pm S.D. of two independent experiments. (C) HpVAL-4 binds cholesterol in vitro. Purified HpVAL-4 protein (100 pmol) was incubated with the indicated concentration of [³H]-cholesterol in the presence (HpVAL-4 + 400 pmol cholesterol) or absence of unlabeled competitor ligand (HpVAL-4). The previously determined Pry1 activity is also shown.

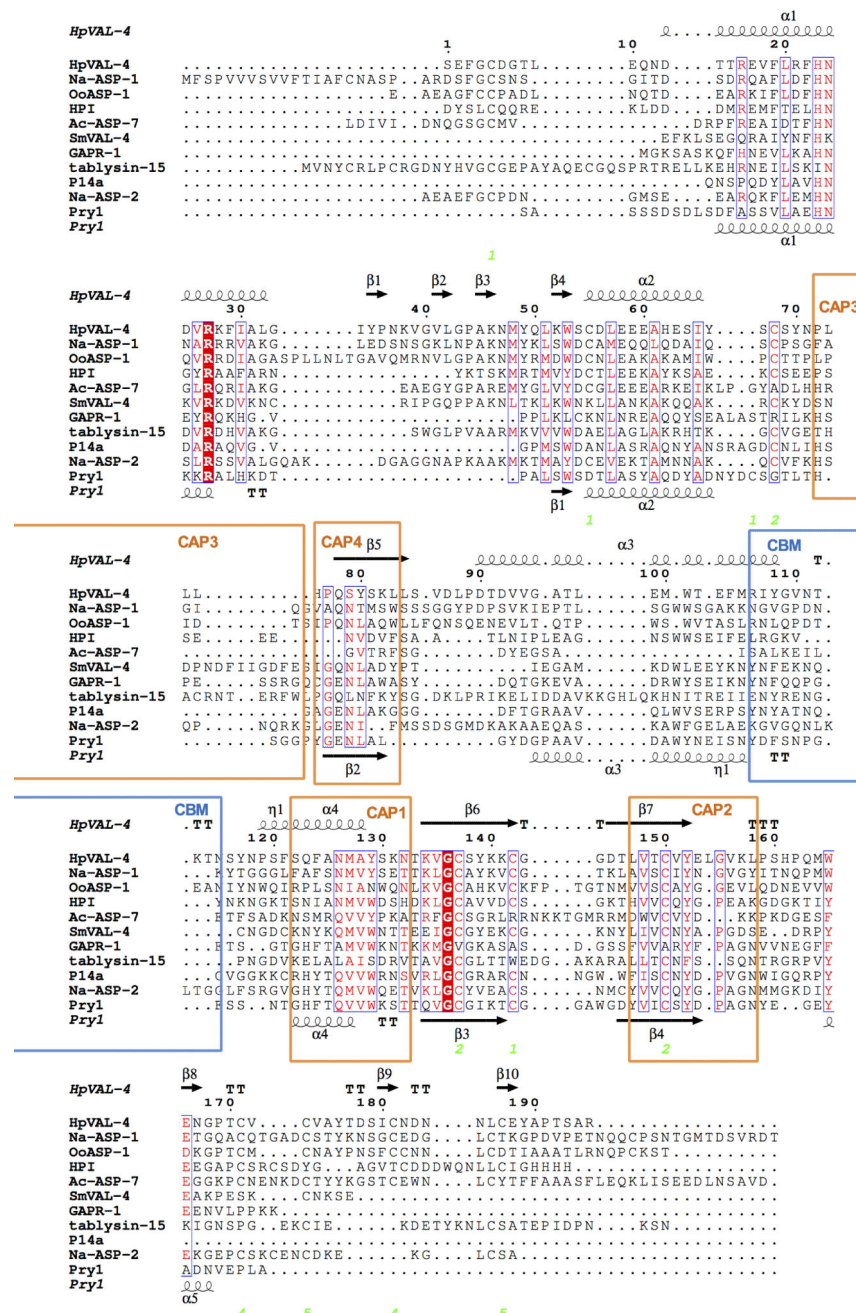


Fig. 4. Comparison of *Heligmosomoides polygyrus* Venom Allergen-like Protein-4 (HpVAL-4) with selected members of its superfamily. The sequences were aligned with clustalW2 and the secondary structural features were illustrated with the coordinates of HpVAL-4 and Pryn1 using ESPript (Gouet et al., 2003). The different secondary structure elements shown are alpha helices (α), 3₁₀-helices (η), beta strands (β), and beta turns (TT). Identical residues are shown in red shading, and conserved residues are in red text. The locations of the cysteine residues involved in disulfide bonds are numbered in green. The location of the caveolin binding motif (CBM) loop is shown in blue bars and the signature cysteine-rich secretory

protein (CRISP) motifs are identified with orange bars. The representative structures are Na-ASP-2 (Asojo et al., 2005), Pry1 (Darwiche et al., 2016), Na-ASP-1 (Asojo, 2011), tablysin-15 (Ma et al., 2011), Golgi-Associated plant Pathogenesis Related protein-1, GAPR-1 (van Galen et al., 2012), *Ostertagia ostertagi* activation-associated secreted protein-1, OoASP-1 (Borloo et al., 2013), *Ancylostoma caninum* Ancylostoma secreted protein-7, Ac-ASP-7 (Osman et al., 2012), *Schistosoma mansoni* Venom Allergen-Like Protein-4, SmVAL4, (Kelleher et al., 2015), and *Solanum lycopersicum* pathogenesis-related protein, P14A (Fernandez et al., 1997).

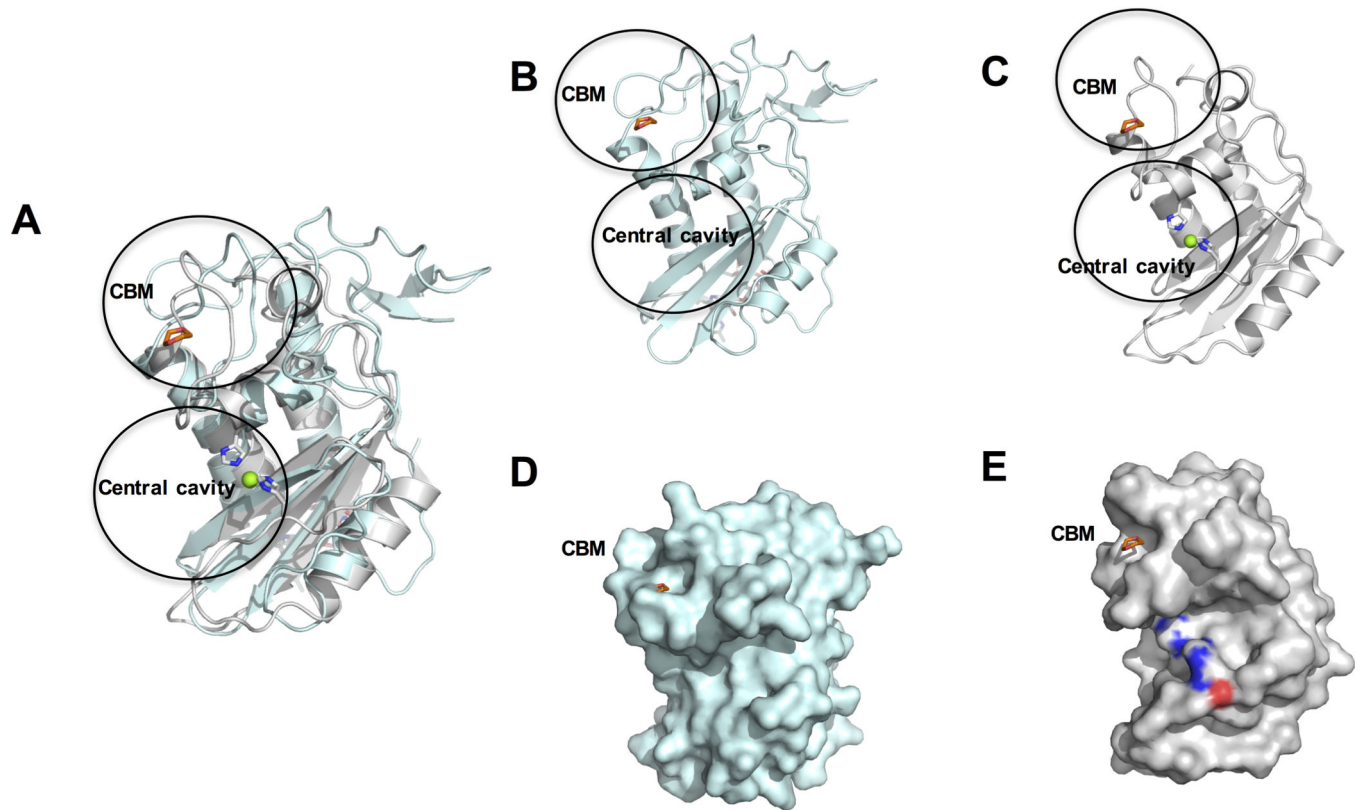


Fig. 5. Comparison of *Heligmosomoides polygyrus* Venom Allergen-like Protein-4 (HpVAL-4) with pathogen-related yeast protein 1 (Pry1). (A) The superposed ribbon structure of HpVAL-4 (cyan) and Pry1 (gray) reveals the conformational flexibility of the caveolin binding motif (CBM) which contains the 1,2-dioxane from the Pry1 structure (shown in red). The central histidines that coordinate cations in Pry1 are colored by elements with blue for N, white for C, red for O. Mg^{2+} is shown as a green sphere. Ribbon diagrams of the same view of (B) HpVAL-4 and (C) Pry1. The sizes of the cavities are evident from the surface plot of the same view of (D) HpVAL-4 and (E) Pry1.

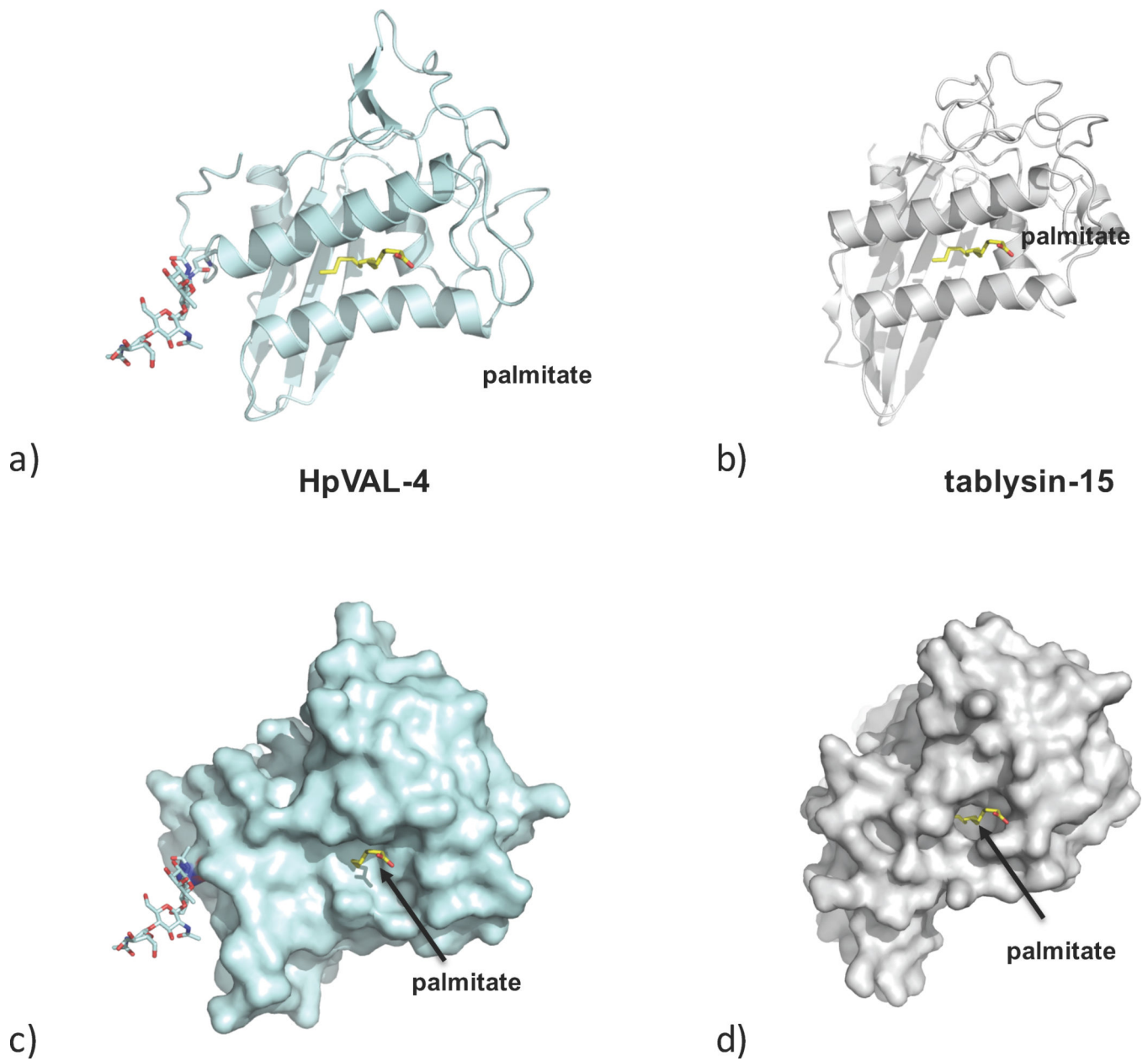


Fig. 6. The palmitate binding cavity. (A) Ribbon diagram of the putative palmitate-binding cavity of *Heligmosomoides polygyrus* Venom Allergen-like Protein-4 (HpVAL-4) based on (B) the palmitate binding of tablysin-15. Surface representations of same view of the palmitate binding cavity of (C) HpVAL-4 and (D) tablysin-15, with palmitate shown as yellow sticks and the glycosylation site on HpVAL-4 as other coloured sticks.

Table 1

Data collection and refinement statistics for *Heligmosomoides polygyrus* Venom Allergen-like Protein-4 (HpVAL-4).

Data collection	HpVAL-4
Wavelength	0.15418 nm
Resolution range (Å)	40.88 – 1.99 (2.061 – 1.99)
Space group	P_1
Unit cell	a = 49.5596 Å b = 61.5645 Å c = 74.8188 Å $\alpha = 111.595^\circ$ $\beta = 90.14^\circ$ $\gamma = 113.475^\circ$
Total reflections	351786 (23932)
Unique reflections	48534 (4696)
Multiplicity	7.2 (7.3)
Completeness (%)	95.36 (92.93)
Mean I / sigma(I)	18 (11.3)
Wilson B-factor	16.45
<i>R</i> -merge	0.139 (0.700)
<i>R</i> -meas	0.156 (0.762)
<i>R</i> -pim	0.084 (0.421)
CC _{1/2}	0.996 (0.961)
Reflections used in refinement	48531 (4696)
Reflections used for R-free	2462 (225)
R-work	0.1748 (0.1824)
R-free	0.2231 (0.2702)
Number of non-hydrogen atoms	6464
macromolecules	5921
ligands	180
solvent	363
Protein residues	749
RMS (bonds)	0.009 Å
RMS (angles)	1.39 °
Ramachandran favored (%)	97.71
Ramachandran allowed (%)	2.29
Ramachandran outliers (%)	0.00
Rotamer outliers (%)	0.15
Clashscore	4.05
Average B-factor	17.84
macromolecules	17.50
ligands	25.31
solvent	19.72

Statistics for the highest resolution shell are shown in parentheses.

RMSD, root-mean-square deviation; CC, correlation coefficient.